nature astronomy

ARTICLES

https://doi.org/10.1038/s41550-021-01339-7

Check for updates

Spin state and moment of inertia of Venus

Jean-Luc Margot[1,2]✉, Donald B. Campbell[3], Jon D. Giorgini[4], Joseph S. Jao[4], Lawrence G. Snedeker[4], Frank D. Ghigo[5] and Amber Bonsall[5]

Fundamental properties of the planet Venus, such as its internal mass distribution and variations in length of day, have remained unknown. We used Earth-based observations of radar speckles tied to the rotation of Venus obtained in 2006–2020 to measure its spin axis orientation, spin precession rate, moment of inertia and length-of-day variations. Venus is tilted by 2.6392 ± 0.0008 deg (1σ) with respect to its orbital plane. The spin axis precesses at a rate of 44.58 ± 3.3 arcsec per year (1σ), which gives a normalized moment of inertia of 0.337 ± 0.024 and yields a rough estimate of the size of the core. The average sidereal day on Venus in the 2006–2020 interval is 243.0226 ± 0.0013 Earth days (1σ). The spin period of the solid planet exhibits variations of 61 ppm (~20 min) with a possible diurnal or semidiurnal forcing. The length-of-day variations imply that changes in atmospheric angular momentum of at least ~4% are transferred to the solid planet.

Venus is Earth's nearest planetary neighbour and closest analogue in the Solar System in terms of mass, radius and density. However, Venus remains enigmatic on a variety of fundamental levels: the size of its core is unknown[1], whether the core is solid or liquid is uncertain[2,3] and estimates of its average spin period are discordant[4–6]. Venus is also distinctive because of its 243-day retrograde rotation and 4-day atmospheric superrotation, neither of which is fully understood[7–9]. High-precision measurements of the spin state enable progress in all these areas.

The polar moment of inertia provides an integral constraint on the distribution of mass in a planetary interior: $C = \int_V \rho r^2 \mathrm{d}V$, where the volume integral includes the mass density ρ at each point and the square of the distance r from the spin axis. Along with bulk density, the moment of inertia is arguably the most important quantity needed to determine the internal structure of a planetary body. In particular, it can be used to place bounds on the size of the core, which is essential in understanding a planet's thermal, spin and magnetic evolutionary histories. Seismology, which has been conducted for Earth, Moon and Mars, provides a powerful probe of planetary interiors, but is considered 'a distant goal' for Venus[10] owing to the planet's extreme surface temperature (~740 K) and pressure (~90 atm).

Gravitational torques from the Sun result in a precession of the spin axis, which is similar to the motion of a spinning top. The rate of precession is inversely proportional to the polar moment of inertia[11]:

$$\frac{\mathrm{d}\psi}{\mathrm{d}t} = \frac{3}{2}\left(\frac{n^2}{\omega}\right) J_2 \left(\frac{MR^2}{C}\right) \cos\theta, \qquad (1)$$

where n is the orbital mean motion, ω is the spin rate, J_2 is the second-degree coefficient in the spherical harmonic expansion of the gravity field, M is the mass, R is the radius and θ is the obliquity or angular separation between spin and orbit poles. Measurements of the spin precession rates of Earth (50.2877 arcsec yr^{-1}) and Mars (7.576 arcsec yr^{-1}) yield $C/MR^2 = 0.3307$ (ref. [12]) and $C/MR^2 = 0.3662$ (ref. [13]), respectively. The predicted precession rate of Venus for a nominal $C/MR^2 = 0.336$ is 44.75 arcsec yr^{-1}, where we have used $n = 585.17$ deg yr^{-1} (ref. [14]), $\omega = 541.06$ deg yr^{-1}, $J_2 = 4.40454 \times 10^{-6}$ (ref. [15]) and $\theta = 2.639$ deg. This value is in good agreement with a previous estimate[16] and implies a precession cycle of ~29,000 yr.

Although the predicted precession rate of Venus is similar to that of Earth, the motion of the spin pole in inertial space is only 2.06 arcsec yr^{-1} because of Venus's small obliquity. Detection of the precession was out of reach of the 1990–1994 Magellan spacecraft mission despite its extensive radar coverage with resolution as fine as 100 m (ref. [17]). The best Magellan estimates of the spin axis orientation from analysis of radar data and gravity data have uncertainties of 46 arcsec (ref. [4]) and 14 arcsec (ref. [15]), respectively. If a future mission were to measure the spin axis orientation with infinite precision at an epoch circa 2040, the measured precession excursion of ~100 arcsec since the Magellan epoch would be determined with 14 arcsec errors at best, or 14% uncertainties, which is not geophysically useful. Likewise, if a future orbiter with a 5-year duration were to measure the inertial positions of landmarks with 30 m precision, it would detect the ~10 arcsec precession over the mission duration, which corresponds to a maximum displacement of ~300 m, with 10% uncertainties at best. A useful measurement could be obtained with telemetry data from multiple landers, as in the case of Mars, but the technical challenge and cost of this endeavour make it improbable in the foreseeable future.

Measurements of the average spin period of Venus with <1% precision were first obtained by tracking the positions of surface features detectable in Earth-based radar images that spanned multiple conjunctions[18–21]. The most precise value to date was obtained by analysing the positions of hundreds of landmarks detectable in Magellan spacecraft radar images recorded in the early 1990s, which resulted in a ~500-day-average spin period estimate of 243.0185 ± 0.0001 d (ref. [4]). Certain features observed in Magellan images were also detected in Venus Express spacecraft images obtained circa 2007, enabling a ~16-year-average spin period estimate of 243.023 ± 0.001 d (ref. [5]). Recent measurements of the positions of surface features in Earth-based radar images obtained between 1988 and 2017 yielded a ~29-year-average spin period estimate of 243.0212 ± 0.0006 d (ref. [6]). None of these estimates were of sufficient precision to detect either sidereal length-of-day (LOD) fluctuations or the precession of the spin axis.

[1]Department of Earth, Planetary & Space Sciences, UCLA, Los Angeles, CA, USA. [2]Department of Physics & Astronomy, UCLA, Los Angeles, CA, USA. [3]Department of Astronomy, Cornell University, Ithaca, NY, USA. [4]Jet Propulsion Laboratory, Pasadena, CA, USA. [5]National Radio Astronomy Laboratory, Green Bank, WV, USA. ✉e-mail: jlm@epss.ucla.edu

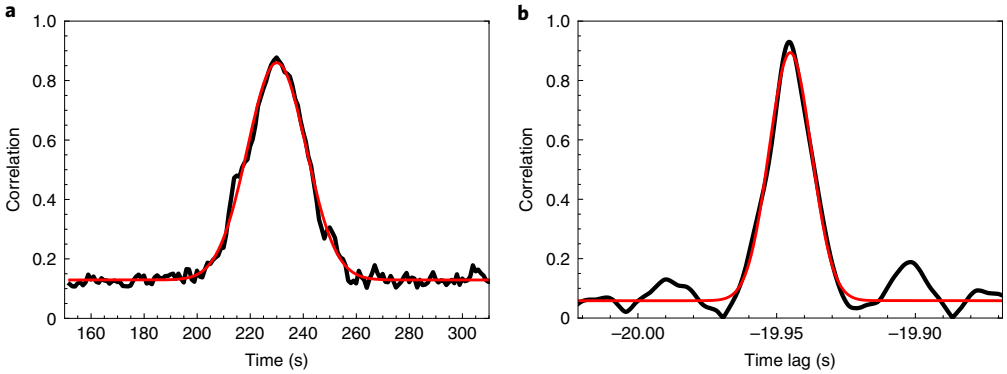

Fig. 1 | Space-time correlation of Venus radar speckles. Representative functions obtained by cross-correlating Venus radar echoes recorded at Goldstone, California, and Green Bank, West Virginia, on 26 November 2016. Gaussian fits are shown in red. **a**, Time evolution of the maximum in the cross-correlation function with echo time series decimated to a sampling rate of 200 Hz. The time of the correlation maximum represents the epoch at which the speckle trajectory sweeps over both antennas and is diagnostic of spin axis orientation. **b**, Cross-correlation of echo time series with 5,000 Hz sampling rate and 5 ms moving average at the time of the correlation maximum shown in **a**. The time lag corresponding to the correlation maximum is diagnostic of the instantaneous spin rate. Successive measurements of this time lag yield the estimates and ~5 ppm fractional uncertainties listed in Table 1.

The maintenance of a 243-day retrograde spin requires explanation because solid body tides raised by the Sun would synchronize the spin of Venus to its 225-day orbital period in the absence of other forces[22,23]. Gold and Soter[24] and others[25–27] proposed that solar torques on a thermally induced atmospheric tide might counteract the solid-body torques and stabilize the spin. In this process, atmospheric mass decreases on the hotter afternoon side of the planet and increases on the colder morning side. This imbalance creates an atmospheric bulge that leads the sub-solar point, whereas the bulge due to tides raised on the solid body lags the sub-solar point. The opposing solar torques may therefore stabilize the spin rate. The solid-body torque is relatively independent of the spin rate, but the strength of the torque on the atmospheric bulge has a semidiurnal dependence[24–26]. It is thought that the spin rate settles where the two torques balance each other. However, the magnitude of variations around the equilibrium and the nature of the response to departures from equilibrium have not been elucidated.

With a spin rate controlled by a thermally driven atmospheric tide, the rotation of the planet likely changes as a result of variations in albedo[7], orbital eccentricity[28], insolation, climate and weather. The insolation changes by 3% as Venus revolves around the Sun with its current eccentricity of 0.007 and by 15% with the long-term average eccentricity of 0.035 (ref. [28]). The planet may therefore exhibit daily and seasonal fluctuations in LOD superposed on a complex spin rate evolution on longer timescales.

Atmospheric angular momentum (AAM) on Earth varies by tens of percent[29] and results in LOD variations on the order of milliseconds. With its massive atmosphere, Venus has an estimated AAM value ($L \approx 2.9 \times 10^{28}\,\mathrm{kg\,m^2\,s^{-1}} \pm 30\%$)[8] that is ~180 times larger than Earth's, and the atmospheric fraction of total planetary angular momentum is ~60,000 times larger than Earth's. If a fraction ϵ of AAM is transferred to the solid planet, the rotation period P changes by $\Delta P/P = -\epsilon L/C\omega$. For Venus, $\Delta P \approx -9.4\epsilon$ h. Peak-to-peak estimates of AAM-induced LOD variations based on Global Circulation Model (GCM) simulations currently span at least two orders of magnitude, with values of ϵ ranging from below ~0.1% (refs. [30,31]) on diurnal timescales to above ~15% (ref. [32]) on decadal timescales.

Observations. We obtained high-precision measurements of the instantaneous spin state of Venus with a radar speckle tracking technique that requires two telescopes and does not involve imaging (see 'Radar speckle tracking' in Methods). We used the 70 m antenna (DSS-14) at Goldstone, California (35.24° N, −116.89° E), and transmitted a circularly polarized monochromatic signal at a frequency of 8,560 MHz ($\lambda = 3.5$ cm) and power of ~200–400 kW. Radar echoes were recorded at DSS-14 and also at the 100 m Green Bank Telescope (GBT) in West Virginia (38.24° N, −79.84° E) with fast sampling systems[33].

Radar echoes from solid surfaces are speckled. The radar speckles are tied to the rotation of Venus and sweep over the surface of the Earth with a trajectory that is occasionally aligned with the two telescopes (Extended Data Figs. 1 and 2). We cross-correlated the echo time series received at each telescope and obtained strong correlations that lasted ~30 s (Fig. 1). The epoch at which the high correlation occurs is diagnostic of the spin axis orientation. The time lag at which the correlation is at a maximum yields a measurement of the instantaneous spin period.

We attempted to observe Venus on 121 instances between 2006 and 2020 (Supplementary Table 1) and were successful on 21 occasions; observing circumstances are reported in Supplementary Table 2. The observing protocol and data reduction technique (see 'Observing protocol' and 'Data reduction technique' in Methods) closely followed those used for similar measurements at Mercury[34,35] that were confirmed at the 1% level by subsequent spacecraft observations[36].

We fit Gaussians to the correlation functions to obtain estimates of the epochs of correlation maximum $\hat{t}$. We also obtained estimates of the time lags $\hat{\tau}$ that maximize the correlation functions (Fig. 1 and Table 1). With large signal-to-noise ratios, Gaussian centroid locations can be determined with a precision that is a small fraction of the widths of the correlation functions[37]. Measurement residuals and spread in consecutive estimates suggest that epochs of correlation maxima and time lags can be determined to precisions of ~0.3 s and ~0.1 ms from initial widths of ~10 s and ~7 ms, respectively. We used the $\hat{t}$ and $\hat{\tau}$ observables to determine the instantaneous spin state of Venus (see 'Conversion of observables to spin state estimates' in Methods).

Spin axis orientation, precession and moment of inertia. The velocity vector of the speckle pattern lies in the plane perpendicular to the component of the spin vector that is perpendicular to the line of sight. The correlation of Goldstone and GBT radar echoes is large only when the antenna separation vector that is projected perpendicular to the line of sight, or projected baseline, lies in the same plane. Correlation epoch measurements provide tight constraints

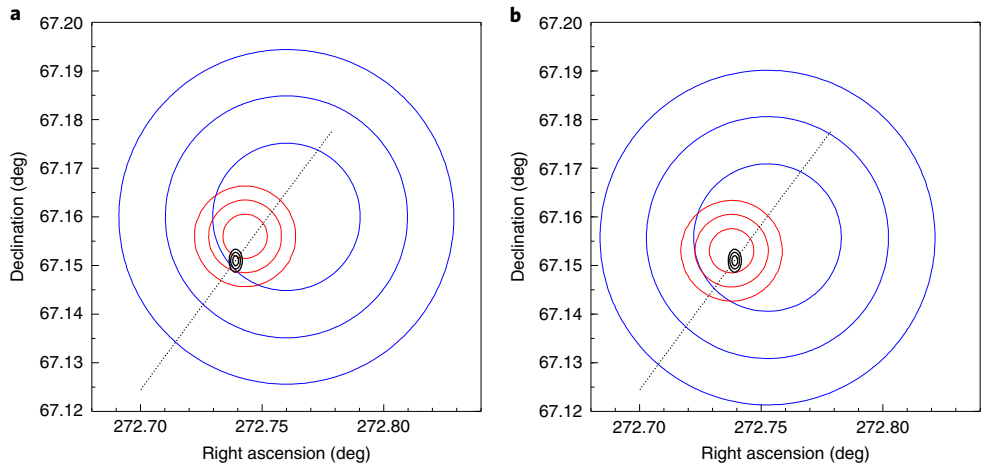

Fig. 2 | Spin axis orientation of Venus. The spin axis orientation of Venus is shown with 1σ, 2σ and 3σ uncertainties (two-dimensional confidence intervals at 68.3%, 95.4% and 99.7% levels, respectively). The epoch J2000.0 solution based on Goldstone-GBT observations is shown in black. The Magellan solutions of Davies et al.[4] and Konopliv et al.[15] are shown in blue and red, respectively. The black dotted line represents the trace of the spin axis orientation on the celestial sphere as a result of spin precession between 1950 and 2050. **a**, Magellan solutions as published by Davies et al.[4] and Konopliv et al.[15]. **b**, Magellan solutions precessed to epoch J2000.0 from the mid-point of the corresponding observation intervals (January 1991 and September 1993, respectively).

on the component of the spin that is perpendicular to the line of sight and loose constraints on the orthogonal component. As a result, each epoch measurement delineates a narrow error ellipse for the orientation of the spin axis on the celestial sphere. We obtained intersecting error ellipses by observing Venus at a variety of orientations (Extended Data Fig. 3).

We used the epochs of correlation maxima (Table 1) with uniform uncertainties in a three-parameter least-squares fit to estimate the spin axis orientation of Venus as well as its precession rate. The first two adjustable parameters are the right ascension (RA) and declination (dec.) of the spin axis in the equatorial frame of J2000.0. The third adjustable parameter is the normalized moment of inertia C/MR^2, with precession modelled according to equation (1). Post-fit residuals have a standard deviation of 0.32 s and their distribution is unremarkable (Supplementary Fig. 1). We estimated confidence intervals with 2,000 bootstrap trials, which confirmed the robustness of the fit results with respect to inclusion or exclusion of certain data points. Results are listed in Table 2.

The spin axis orientation of Venus is determined with an overall precision of 2.7 arcsec, which improves upon the Magellan estimates by a factor of 5–15 (Fig. 2). At first glance, our estimates are only marginally consistent with the Magellan estimates. However, the spin axis orientation measured by Magellan in the early 1990s is not directly comparable to our solution, which has a reference epoch of J2000.0. If we use our estimate of the precession rate and precess the Magellan estimates to epoch J2000.0, we find that our values fall well within the Magellan 1σ uncertainty contours (Fig. 2).

Our improved value of the obliquity of Venus is 2.6392 ± 0.0008 deg (1σ), for which we have used a recent determination of the orbital plane orientation with RA = 278.007642 deg and dec. = 65.566999 deg (ref. [14]). The origin and maintenance of the obliquity has been linked to planetary perturbations, core–mantle friction and atmospheric torques[7,38,39]. If the core is liquid, the obliquity estimate can be used to place bounds on the viscosity or ellipticity of the core, provided that atmospheric torques are modelled accurately[7].

The distribution of normalized moments of inertia from the bootstrap analysis suggests residual uncertainties of 7% with the data obtained to date (Extended Data Fig. 4). The results are not yet sufficient to rule out certain classes of interior models, whose normalized moments of inertia computed in a recent study[2] span the range 0.327–0.342. Nevertheless, the best-fit value of the moment of inertia factor combined with knowledge of the bulk density ($\rho = 5242.8\,\mathrm{kg\,m^{-3}}$) enable a crude estimate of the size of the core of Venus with a two-layer uniform-density model (see 'Two-layer interior structure model' in Methods). We find a core radius of approximately 3,500 km (58% of the planetary radius) with large (>500 km) uncertainties owing to both model limitations and current uncertainties in C/MR^2.

Spin period and length-of-day variations. We used the time lag measurements to compute the spin period of Venus at each observation epoch (Table 1). The data show that Venus exhibits substantial LOD variations (Fig. 3). We reject the hypothesis of a constant spin period with high confidence (probability $<< 10^{-16}$) because a model with constant spin period yields a large sum of squares of residuals (SSR = 620). In addition, we find that published values of Venus's average spin rate[4–6] are inconsistent with most of our instantaneous spin period measurements.

Our data set spans almost 15 years and includes 21 measurements with an average fractional uncertainty of 5 ppm. The median value of our measurements provides a robust estimate of the average length of day on Venus, $P = 243.0226 \pm 0.0013$ d (1σ), where the error bars are obtained by bootstrap resampling (see 'Estimate of average spin period' in Methods). Natural variability around the mean is at least ± 0.0047 d (1σ). Our improved determinations of the spin axis orientation, precession rate and spin period form the basis of a recommended orientation model for Venus (Supplementary Information). This model and the model currently in use[4] yield differences in the predicted inertial positions of equatorial landmarks that grow by ~1 km per year. Stochastic LOD variations over a 10-year period contribute an additional uncertainty of ± 3.3 km (1σ), which will complicate the establishment of new geodetic control networks and the measurement of the spin precession from orbital or landed platforms (Supplementary Information).

The fractional excursion in instantaneous spin rate observed to date is 61 ppm, which corresponds to variations in spin period of 0.015 d or 21 min. In seven instances, we observed Venus on consecutive days and measured variations ranging between 2 ppm and

Table 1 | Measurements of the instantaneous spin state of Venus

Date	Epoch (MJD)	*A*	*w* (s)	Time lag (s)	ϵ (ppm)	*P* (days)
060128	53763.69074757	0.593	4.70	−149.224656	6.09	243.01724
060129	53764.69293247	0.622	5.11	−142.602992	7.42	243.02106
060207	53773.69201430	0.573	6.24	−95.544513	6.57	243.01721
060214	53780.67533999	0.594	12.52	−74.199631	3.93	243.02289
060219	53785.65987182	0.696	9.66	−63.745660	4.44	243.02168
090614	54996.76400084	0.709	9.27	−20.401318	3.07	243.01596
090801	55044.63200521	0.583	13.98	−17.883815	5.76	243.01594
120310	55996.01816745	0.693	4.85	−18.228874	4.44	243.02257
120311	55997.01549785	0.615	5.32	−18.748452	3.71	243.02468
120314	56000.00753916	0.654	5.28	−20.327400	7.44	243.02073
120315	56001.00490798	0.663	5.65	−20.860567	5.54	243.01651
140312	56728.58912128	0.705	9.73	−36.100686	2.19	243.02960
140314	56730.58274410	0.764	9.81	−34.453769	2.73	243.02925
140315	56731.57957689	0.807	9.63	−33.652202	2.41	243.03075
161122	57714.87788177	0.693	12.90	−19.417283	4.60	243.02861
161125	57717.87004808	0.760	11.75	−19.821632	4.01	243.02932
161126	57718.86741525	0.779	11.45	−19.945238	3.29	243.02635
190206	58520.68253779	0.562	14.52	−21.925929	5.68	243.02289
190207	58521.67959325	0.564	14.83	−21.846558	4.72	243.02335
190208	58522.67663675	0.568	12.70	−21.759899	5.23	243.02186
200908	59100.52352634	0.497	8.02	−17.088679	4.51	243.01782

The epoch of correlation maximum is reported as a modified Julian date (MJD). It is the centroid of a Gaussian of amplitude *A* and standard deviation *w*. The time lag indicates the time interval for speckles to travel from one station to the other at the corresponding epoch. The reference epochs correspond to arrival times at the GBT, and the negative lag values indicate that Venus speckles travel from west to east. The 1σ fractional uncertainty ϵ that applies to both the time lag and spin period is empirically determined from successive measurements. The last column indicates the instantaneous sidereal spin period in Earth days, after application of small refraction corrections (Table 2).

Table 2 | Spin axis orientation and precession estimates from least-squares fit and bootstrap analysis

Quantity	Least-squares	Bootstrap mean	σ
RA (deg)	272.73911	272.73912	0.0008
Dec. (deg)	67.15105	67.15100	0.0007
$d\psi/dt$ ($''yr^{-1}$)	−44.89	−44.58	3.3
C/MR^2	0.3350	0.3373	0.024
C (10^{37} kg m^2)	5.972	6.013	0.43

Angles refer to epoch J2000.0.

17 ppm with a weighted average value of 9 ± 5 ppm (1σ), which suggests a spin rate of change as large as $d\omega/dt \approx 3.1 \times 10^{-17}$ rad s^{-2} and corresponding torques of $T = C d\omega/dt \approx 1.9 \times 10^{21}$ N m. The LOD variations observed at Venus are three orders of magnitude larger than on Earth, where core–mantle interactions can change the LOD by ~4 ms (46 ppb) on ~20-year timescales[40]. The torques responsible for the LOD variations on Earth are $T_\oplus = C_\oplus d\omega_\oplus/dt \approx 4.3 \times 10^{17}$ N m, where $d\omega_\oplus/dt \approx 5.4 \times 10^{-21}$ rad s^{-2} and $C_\oplus = 8.0 \times 10^{37}$ kg m^2. If Venus has a liquid core, it may experience torques of the same order of magnitude, which would yield $d\omega/dt \approx 10^{-20}$ rad s^{-2}, a factor of 10^3 too small compared to observations. Tidal despinning torques are an order of magnitude smaller. We conclude that changes in AAM are primarily responsible for the LOD variations at Venus. Other contributions to the LOD variations include a ~3 ppm variation at semidiurnal frequencies due to solar torques on Venus's permanent deformation and possibly sub-ppm variations due to core–mantle interactions[31]. The AAM variations are so large that they likely prevent capture in resonances with Earth, a phenomenon that has been hypothesized for decades[7,25,28,41].

If the AAM budget on Venus is 2.9×10^{28} kg m^2 s^{-1} (ref. [8]), the 61 ppm fractional excursion in spin period measured to date provides a lower bound on the fractional change in AAM of $\epsilon = 3.8\%$. The ~9 ppm variations observed on consecutive Earth days correspond to spin period changes of ~3 min and $\epsilon = 0.6\%$. Certain GCM simulations show changes in AAM amounting to $\epsilon = 0.1\%$ or less over half a Venusian day[30,31], which suggests a rate of change in AAM that is ~300 times lower than what we observe. A more recent GCM simulation indicates an ϵ as large as 0.6% over a quarter of a Venusian day[42], or a rate of change that is ~30 times lower than what we observe. Modelling the dynamical state of the Venus atmosphere with quantitative precision is difficult[8] and validation of Venus GCMs is complicated by the fact that few measurements of the internal dynamics of the atmosphere are available. Our measurements provide useful calibration data for GCMs.

Because secular evolution of the spin rate is likely, we tested for the presence of a linear trend in our measurements. The slopes detected in linear regressions with unweighted and weighted uncertainties are not statistically significant, and we are unable to detect a long-term trend in the data obtained to date.

We also examined whether the measurements exhibited periodicities related to the spin (ω), orbital (n) and diurnal ($\omega + n$) frequencies, including ω, n, 2ω, $\omega + n$, $2n$, $\omega + 2n$ and $2\omega + 2n$ (Fig. 3). Although we are currently unable to detect periodicities with confidence or attribute the LOD variations to specific causes, we speculate on possible causes and effects of periodicities at semidiurnal, diurnal or orbital periods that may be present (Supplementary Fig. 7 and Supplementary Tables 5 and 6).

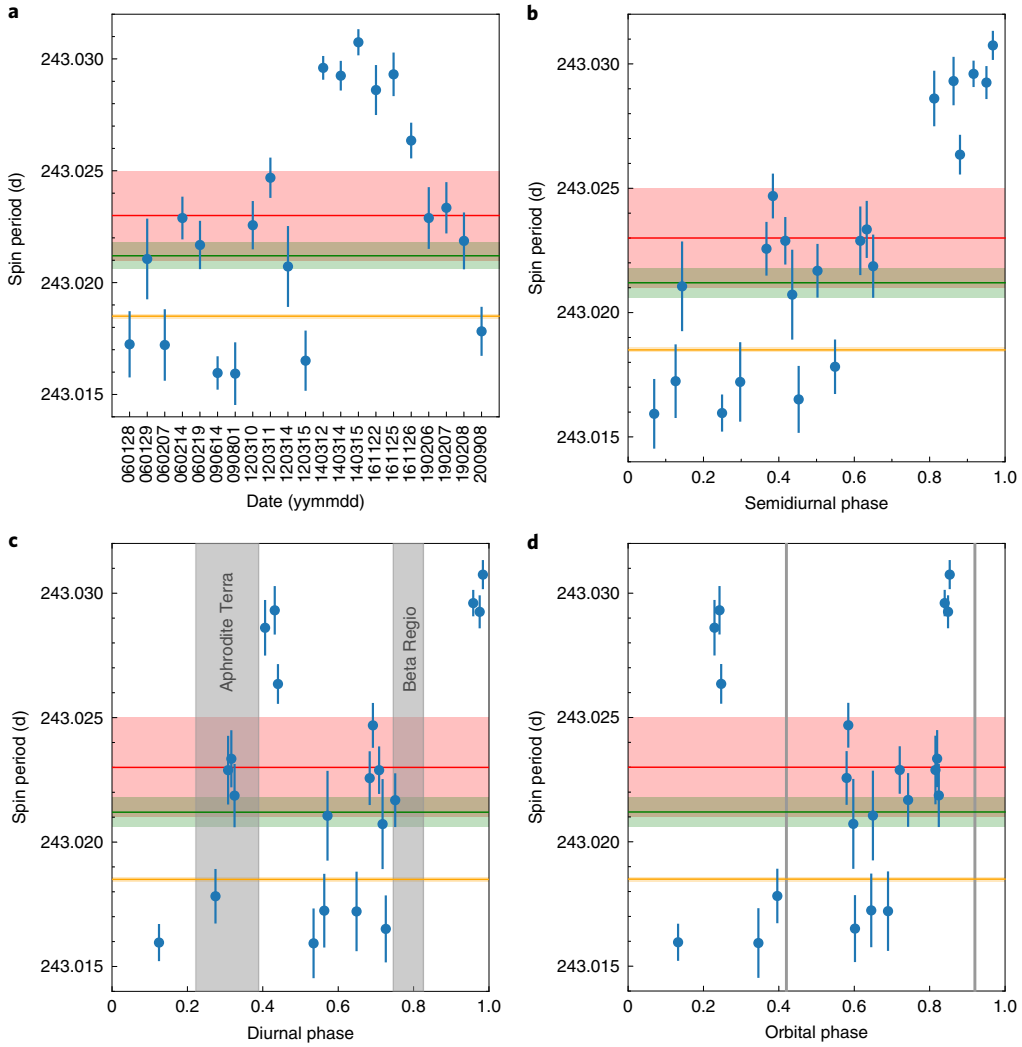

Fig. 3 | Measurements of the instantaneous spin period of Venus. a, Measurements of the instantaneous spin period of Venus shown as blue dots with 1σ error bars. These data are based on time lag measurements of radar speckles observed with Goldstone and the GBT between 2006 and 2020. Horizontal lines and shaded areas show the average spin periods derived from Magellan radar images (1990–1992, orange), Magellan and Venus Express images (1991 and 2007, red) and Earth-based radar images (1988–2017, green). **b**–**d**, Same data folded onto a semidiurnal cycle (-58.4 d) (**b**), diurnal cycle (-116.8 d) (**c**), and orbital cycle (-224.7 d) (**d**). The origin of phase is 2000 February 22 10:43:58 TDB, when the sub-solar longitude is approximately zero. Vertical grey bands and lines indicate local noon over low-latitude highlands and equinoxes, respectively.

The possibility of semidiurnal variations in the AAM budget is intriguing because this period controls the strength of the atmospheric tide[24–26]. If confirmed, this periodicity would require an impulsive release of ~4% of the total AAM twice per Venusian day, with profound consequences for the internal dynamics of the atmosphere. The rotation of Venus would repeatedly slow down over a period of 58.4 d and depart from the equilibrium value while AAM increased. An impulsive release of AAM would provide a restoring torque and spin the solid planet back up. How such a process would operate is unknown.

If diurnal variations in AAM were confirmed instead, one could invoke mountain torques to explain some of the variations. Mountain torques are hypothesized to cause remarkable planetary-scale features observed in the rapidly rotating upper atmosphere that are stationary with respect to the slowly rotating surface[43,44]. The torques affect the rotation rate of the solid body[42], and our data suggest slower rotation after midday over low-latitude highlands. However, the simulations conducted to date suggest diurnal changes in LOD of 2 min (ref. [42]), whereas we observe LOD variations of at least 20 min.

One possible cause of AAM variations on annual timescales is the convective updraught related to Hadley cell circulation, whose location depends on sub-solar latitude[45]. With thermal inertia, the maxima in AAM and minima in spin period would be delayed from the equinoxes (Fig. 3).

Methods

Radar speckle tracking. When Venus is illuminated with a monochromatic radio signal, a large number of individual surface and near-surface elements scatter the signal back towards the observer, where each contribution to the radar echo has a specific amplitude and phase. It is the superposition (complex sum) of these individual responses that gives the radar echo its speckled nature. Because of constructive and destructive interference, the echo power varies in a random-like fashion (Supplementary Fig. 1). However, apart from receiver noise, the received signal is not random but is determined by the distribution and properties of scatterers on the rigid surface of Venus. Therefore, the pattern of speckles is tied to the rotation of Venus and sweeps over the surface of the Earth along a trajectory dictated by the spin state. Green[46,47] described this pattern as frozen corrugations in the reflected wavefront and illustrated it by drawing contours of constant electric field strength moving in the receiver (ground) plane. He also detailed how the motion of the pattern is diagnostic of the target's instantaneous spin state and suggested cross-correlating time series of the electric field amplitudes recorded at

two receiving stations. The speckle coherence conditions and applicability to the measurement of planetary spin states were expanded by Holin[48,49], who also showed that the technique works for arbitrary topography.

The characteristic scale of the speckles is given by the classic diffraction formula $r\lambda/d$, where r is the range to the planet, λ is the wavelength and d is the diameter of the scattering area on the target, on the order of the planetary radius. For Venus ($R=6{,}051.8$ km) observed at $r=0.8$ astronomical units (au) and $\lambda=3.5$ cm, the speckle scale is ~0.7 km. Most of the time, observers located at separate antennas record distinct radar speckle patterns, in which case cross-correlation of the radar echo time series obtained at separate antennas yields low correlation scores. During brief periods (~30 s) on suitable days, the wavefront corrugations follow a trajectory that sweeps over both antennas used in this work (Supplementary Fig. 2), the Goldstone and Green Bank antennas. When this situation arises, large correlation scores (>0.6) are obtained at certain time lags, typically ~20 s. The epoch at which the high correlation occurs is diagnostic of the spin axis orientation. The time lag at which the high correlation occurs yields a measurement of the instantaneous spin period.

The short duration of the high-correlation condition is explained by the speckle size and the length of the projected baseline, that is, the antenna separation vector projected perpendicular to the line of sight. Because the speckle scale (~0.7 km) is so small compared to the projected baseline (~3,000 km), a small (0.01 deg) misalignment of the speckle trajectory with respect to the baseline orientation results in appreciable decorrelation. For an east–west baseline that oscillates daily by ±23 deg with respect to the ecliptic, the high-correlation condition is maintained each day for only ~30 s.

Radar speckle tracking was used to reveal that Mercury's outer core is molten[34] and to measure its moment of inertia and core size[35,50]. The accuracy of the technique was demonstrated by subsequent spacecraft measurements of Mercury's spin axis orientation and amplitude of longitude librations, which are in excellent agreement (1%) with the radar estimates[36].

Observing protocol. We illuminated Venus with monochromatic radiation (8,560 MHz, 450 kW) from the Deep Space Network (DSN) 70 m antenna in Goldstone, California (DSS-14), and we recorded the speckle pattern as it swept over two receiving stations (DSS-14 and the 100 m antenna in Green Bank, West Virginia). The transmitted waveform was circularly polarized (right-circular, IEEE definition), and we recorded the echoes in both right-circular (same sense) and left-circular polarizations (opposite sense). The opposite-sense echo is generally an order of magnitude stronger and was used for the spin state measurements. To compensate for the Earth–Venus Doppler shift, the transmitted waveform was continuously adjusted in frequency by a programmable local oscillator so that the echo centre at the GBT remained fixed at 8,560 MHz. Because the Doppler shift was compensated for reception at the GBT, there was a residual Doppler shift during reception at Goldstone. Differential Doppler corrections were applied with a programmable local oscillator at Goldstone so that the echo centre also remained fixed at 8,560 MHz. At both stations, a positive frequency offset of 2,000 Hz was added in the frequency downconversion chain to prevent the ~350-Hz-wide Venus echo from overlapping with 0 Hz (d.c.).

On any given day, transmission typically occurred for the duration of the round-trip light time to Venus. The receive window started immediately after transmission ended. Transmit times were selected so that the predicted high-correlation epochs were positioned within the receive windows.

During reception, variations in the electric field were detected by the standard low-noise X-band receivers at DSS-14 and GBT. At Goldstone, the signal was converted to intermediate frequencies of 325 MHz and 50 MHz prior to mixing to baseband. At GBT, the signal was converted to intermediate frequencies of 720 MHz and 30 MHz prior to mixing to baseband. During conversion to baseband the in-phase (I) and quadrature (Q) components of the signal were generated. Both I and Q voltages were low-pass filtered, sampled with analogue-to-digital converters and recorded to computer hard drives. For most observations, voltages were low-pass filtered at 1.9 MHz, sampled at 5 MHz by our custom-built Portable Fast Sampler data-taking systems[33] and stored with 4-bit resolution. The 2020 and 2019 observations at the GBT were low-pass filtered at 1.25 MHz, sampled at 6.25 MHz by the Dual Channel Agile Receiver data-taking system and stored with 8-bit resolution.

Data reduction technique. After the observations, we downsampled the data to effective sampling rates f_s between 30 Hz and 5,000 Hz and computed the complex cross-correlation of the Goldstone and GBT signals.

The I and Q samples can be thought of as the real and imaginary parts of a complex signal $\{z(t)\}$, with $z(t)=I(t)+jQ(t)$ and $j=\sqrt{-1}$.

The complex-valued cross-correlation of the signals $\{z_1(t)\}$ and $\{z_2(t)\}$ is given by

$$R_{z_1z_2}(t,\tau) = E[z_1(t)z_2^*(t+\tau)], \quad (2)$$

where t is the time or epoch, τ is the time lag, $E[]$ represents the expectation value operator and * represents the complex conjugate operator. The normalized value of the correlation is obtained with

$$\rho_{z_1z_2}(t,\tau) = \frac{|R_{z_1z_2}(t,\tau)|}{\sqrt{|R_{z_1z_1}(t,0)||R_{z_2z_2}(t,0)|}}, \quad (3)$$

where || is the absolute value operator. As the maximum possible value of the correlation $R_{zz}(t,\tau)$ at each t occurs at $\tau=0$, $\rho_{z_1z_2}(t,\tau)$ is ≤1 for all τ.

The complex cross-correlation $\rho_{z_1z_2}(t,\tau)$ is a two-dimensional correlation function in the variables t and τ. Examples of one-dimensional slices through the peak of the correlation function are shown in Fig. 1. We fit Gaussians to the one-dimensional slices to obtain estimates of the epochs of correlation maximum $\hat{t}$. We also obtained estimates of the time lags $\hat{\tau}$ that maximize the correlation functions.

For epoch correlations, we used $f_s=200$ Hz, or about half the Doppler broadening due to Venus's rotation, and integration times of 4 s, except for the 2020 data for which integration times of 1 s were used owing to reduced phase coherence related to the lack of Doppler compensation on that day. We also obtained correlations with $f_s=200$ Hz after low-pass filtering of the radar echoes with a cut-off frequency set at 10% of the Doppler broadening. We found that the low-pass filtered versions, which have higher overall signal-to-noise ratios, yielded slightly larger correlation values than the unfiltered versions (0.65 compared to 0.59 on average), and we used them in the analysis.

We assigned uniform uncertainties to epoch measurements for two reasons. First, the width of the Gaussian correlates with speckle size and therefore Earth–Venus distance (Supplementary Information). Because certain baseline orientations are observable only at certain distances, non-uniform uncertainties would bias the fit towards certain baseline orientations. Second, complex correlations of the 2012 observations are corrupted, but amplitude correlations are well behaved. We used the amplitude correlations results for the 2012 data, but amplitude correlations have notably narrower Gaussian widths than complex correlations.

For time lag correlations, we used $f_s=5{,}000$ Hz, boxcar averaging to 200 Hz, and non-overlapping integration times of 1 s within ±10 s of the peak, which yielded 21 independent estimates during the high-correlation period. We selected all estimates with a correlation amplitude larger than 0.3, which left 12–21 points per epoch (19 data points on average) and a mean correlation amplitude of 0.58.

The time lags evolve appreciably with time owing to the changing Earth–Venus geometry, and we performed linear regressions of the time lag measurements to produce one estimate of the time lag per epoch. We used 2,000 bootstrap trials to randomly exclude data points from the linear regressions and used the bootstrap means and standard deviations as estimates of the time lags and uncertainties at the reference epochs (Table 1). The intrinsic variability of these estimates estimates is 2–7 ppm and 4 ppm on average.

Certain systematic effects may affect the spin rate measurements. We evaluated the error in spin period determination introduced by the residual uncertainty in spin axis orientation by solving for spin periods at various orientations within the error ellipse. We found that it is <1 ppm for 15 epochs and <2 ppm for the remaining 6 epochs. We evaluated the error introduced by imperfect knowledge of the epoch of correlation maximum by solving for spin periods with epochs modified by the standard deviation of epoch residuals (±0.32 s) multiplied by $\sqrt{N/(N-M)}$ to adjust for the sample standard deviation (here, $N=21$ and $M=3$). We found that it is <3 ppm for 17 epochs and <5 ppm for the remaining 4 epochs, with the largest errors affecting the March 2012 observations. We added the variances due to these errors to the variances due to bootstrap resampling of the time lag measurements to produce spin period uncertainties. The resulting fractional uncertainties range from 2 ppm to 7 ppm with an average value of 5 ppm.

Conversion of observables to spin state estimates. We used the observables $\hat{t}$ and $\hat{\tau}$ to obtain spin state estimates (spin axis orientation and instantaneous spin rates). In these calculations the planet state vectors are furnished by a Navigation and Ancillary Information Facility (NAIF) kernel (de438.bsp) that represents the Jet Propulsion Laboratory planetary ephemeris DE438. The Earth orientation is provided by a NAIF kernel (earth_latest_high_prec.bpc) that includes up-to-date timing and polar motion data. The formalism for predicting the (t,τ) values that yield high correlations is described in detail in Appendix B of ref. [35]. Calculations include time delays that account for light-travel times, general relativistic corrections to the time delays and Lorentz transformations for bounce point conditions[35]. We link the observables $\hat{t}$ and $\hat{\tau}$ to spin state estimates with these predictions and the following procedures.

The space-time positions of the two receiving stations at the epochs of correlation maxima were used to solve for the spin axis orientation that generates similar speckles at both receiving stations. We used a least-squares approach to minimize the residuals between the predicted epochs and the observed epochs. The best-fit spin axis orientation is referred to the epoch J2000.0. The precession model for the spin axis is given by equation (1).

After the spin axis orientation was determined, we used each time lag measurement to determine the instantaneous spin rate at the corresponding epoch, once again based on the similarity requirement for the speckles. We iteratively adjusted the nominal spin rate of -1.4813688 deg d^{-1} by a multiplicative factor until the predicted time lag matched the observed time lag.

The nominal DSN–GBT baseline is 3,260 km in length. In the spin rate problem, it is the projected baseline that is relevant, that is, the baseline component

that is perpendicular to the line of sight. Because of the displacement of the light rays due to refraction in the Earth's atmosphere, the effective projected baseline differs from the nominal value. A correction factor for refraction within Earth's atmosphere (Table 2) was applied to the spin rate at each observation epoch. The formalism for this calculation is described in detail in Appendix C of ref. [35]. However, these corrections are small. The worst-case correction at the largest zenith angle of ~65° is ~15 m for a projected baseline of ~3,257 km, that is, a fractional change of 4 ppm.

Passage through Venus's atmosphere retards light rays to both telescopes by <1 microsecond, which is much smaller than our uncertainties. Our measurements are robust with respect to refraction within Venus's atmosphere because the light rays to each scatterer follow essentially identical paths during the high-correlation epoch. The differences in incidence angles for scatterers observed by DSN and GBT always differ by <6 arcsec and most differ by <2.5 arcsec, such that the light rays received at DSN and GBT experience essentially identical atmospheric delays.

One-way absorption through the atmosphere of Venus at the sub-Earth point is ~5.62 dB at X band[51], which effectively decreases our signal-to-noise ratio by a factor of ~10 compared to that of a hypothetical atmosphereless Venus.

Two-layer interior structure model. We considered a two-layer uniform-density model to provide a crude estimate of the core size. We emphasize the limitations of such a model. The large pressures inside Venus result in density profiles that vary with depth, which violate the uniform density assumptions. The two-layer model therefore yields biased estimates.

The three unknowns are the bulk density of the core, the bulk density of the mantle and the radius of the core. Dumoulin et al.[2] used a rescaled version of the Preliminary Reference Earth Model[52] to estimate Venus core densities. Perhaps in part as a result of this choice, all of their models with C/MR^2 in the range 0.327–0.342 have core densities within 1% of 10,358 kg m^{-3}. We set the core density to this value and solved for the other two unknowns, being mindful that other assumptions on core density would yield different results. We found a core radius of 3,508 km (58% of the planetary radius) and a mantle density of 4,006 kg m^{-3}. However, current uncertainties in C/MR^2 result in large (500 km) uncertainties in core size. For comparison, the Earth's core radius is 3,480 km (55% of Earth's equatorial radius) and mantle density is ~4,400 kg m^{-3}.

Estimate of average spin period. Our data set spans almost 15 years and includes 21 measurements of the instantaneous spin period with an average fractional uncertainty of 5 ppm. The median of our instantaneous measurements, $P = 243.0226$ d, provides a robust estimate of the average spin period, which we confirmed with 10,000 bootstrap trials. In these trials, mock data sets were created by selecting 21 data points at random, with replacement. These trials demonstrate robustness with respect to inclusion or exclusion of certain data points. For each trial, we computed the weighted average and the median of the spin period. The distribution of weighted averages yields 243.0227 ± 0.0013 d (95% confidence interval of 243.0202–243.0252 d) and the distribution of medians yields 243.0224 ± 0.0012 (95% confidence interval of 243.0207–243.0247 d), with a median of 243.0226 d. We adopt 243.0226 ± 0.0013 d (1σ) as our best estimate of the average spin period of Venus in the interval 2006–2020.

Our estimate differs substantially from the ~500-day-average Magellan estimate of 243.0185 ± 0.0001 d (ref. [4]), is almost identical to the ~16-year-average spin period estimate of 243.023 ± 0.001 d of Mueller et al.[5] and is marginally consistent with the ~29-year-average spin period estimate of 243.0212 ± 0.0006 d of Campbell et al.[6].

Identification of periodicities. We tested for the presence of periodicities by computing Lomb periodograms[53] and phase dispersion minima (PDM)[54]. We tested thousands of trial periods between 1 d and 5,400 d (Supplementary Fig. 5). These analyses yielded ranked lists of candidate periods, the first ten of which were examined and found to have no obvious physical significance (Supplementary Tables 3 and 4). Phase-folding the data with the candidate periods did not result in convincing patterns (Supplementary Fig. 6), suggesting that these candidate periodicities are spurious detections from a noisy and sparsely sampled data set.

We also examined whether the measurements exhibited periodicities related to the spin (ω), orbital (n) and diurnal ($\omega + n$) frequencies, including ω, n, 2ω, $\omega + n$, $2n$, $\omega + 2n$ and $2\omega + 2n$. The semidiurnal period ranked highest according to both the Lomb periodogram (Supplementary Fig. 7 and Supplementary Table 5) and the θ_{PDM} statistic, which also favoured the diurnal period and, to a lesser extent, the orbital period (Supplementary Table 6).

Data availability

The data sets generated and/or analysed during the current study are available from the corresponding author upon reasonable request.

Code availability

Software used to obtain and process the radar echo time series is available upon request by contacting the corresponding author.

Received: 14 October 2020; Accepted: 26 February 2021;
Published online: 29 April 2021

References

1. Smrekar, S. E., Davaille, A. & Sotin, C. Venus interior structure and dynamics. *Space Sci. Rev.* **214**, 88 (2018).
2. Dumoulin, C., Tobie, G., Verhoeven, O., Rosenblatt, P. & Rambaux, N. Tidal constraints on the interior of Venus. *J. Geophys. Res. Planets* **122**, 1338–1352 (2017).
3. O'Rourke, J. G., Gillmann, C. & Tackley, P. Prospects for an ancient dynamo and modern crustal remanent magnetism on Venus. *Earth Planet. Sci. Lett.* **502**, 46–56 (2018).
4. Davies, M. E. et al. The rotation period, direction of the North Pole, and geodetic control network of Venus. *J. Geophys. Res. Planets* **97**, 13141–13151 (1992).
5. Mueller, N. T., Helbert, J., Erard, S., Piccioni, G. & Drossart, P. Rotation period of Venus estimated from Venus Express VIRTIS images and Magellan altimetry. *Icarus* **217**, 474–483 (2012).
6. Campbell, B. A. et al. The mean rotation rate of Venus from 29 years of Earth-based radar observations. *Icarus* **332**, 19–23 (2019).
7. Yoder, C. F. in *Venus II: Geology, Geophysics, Atmosphere, and Solar Wind Environment* (eds Bougher, S. W. et al.) 1087–1124 (Univ. of Arizona Press, 1997).
8. Sánchez-Lavega, A., Lebonnois, S., Imamura, T., Read, P. & Luz, D. The atmospheric dynamics of Venus. *Space Sci. Rev.* **212**, 1541–1616 (2017).
9. Horinouchi, T. et al. How waves and turbulence maintain the super-rotation of Venus' atmosphere. *Science* **368**, 405–409 (2020).
10. *Roadmap for Venus Exploration* (Venus Exploration Assessment Group, 2019).
11. Kaula, W. M. *An Introduction to Planetary Physics: The Terrestrial Planets* (Wiley, 1968).
12. Williams, J. G. Contributions to the Earth's obliquity rate, precession, and nutation. *Astron. J.* **108**, 711–724 (1994).
13. Folkner, W. M., Yoder, C. F., Yuan, D. N., Standish, E. M. & Preston, R. A. Interior structure and seasonal mass redistribution of Mars from radio tracking of Mars Pathfinder. *Science* **278**, 1749–1751 (1997).
14. Standish, E. M. & Williams, J. G. in *Explanatory Supplement to the Astronomical Almanac* 3rd edn (eds Urban, S. E. & Seidelmann, P. K.) Ch. 8 (University Science Books, 2013).
15. Konopliv, A. S., Banerdt, W. B. & Sjogren, W. L. Venus gravity: 180th degree and order model. *Icarus* **139**, 3–18 (1999).
16. Cottereau, L. & Souchay, J. Rotation of rigid Venus: a complete precession-nutation model. *Astron. Astrophys.* **507**, 1635–1648 (2009).
17. Saunders, R. S. et al. Magellan mission summary. *J. Geophys. Res. Planets* **97**, 13067–13090 (1992).
18. Shapiro, I. I., Campbell, D. B. & de Campli, W. M. Nonresonance rotation of Venus. *Astrophys. J. Lett.* **230**, L123–L126 (1979).
19. Zohar, S., Goldstein, R. M. & Rumsey, H. C. A new radar determination of the spin vector of Venus. *Astron. J.* **85**, 1103–1111 (1980).
20. Shapiro, I. I., Chandler, J. F., Campbell, D. B., Hine, A. A. & Stacy, N. J. S. The spin vector of Venus. *Astron. J.* **100**, 1363–1368 (1990).
21. Slade, M. A., Zohar, S. & Jurgens, R. F. Venus: improved spin vector from Goldstone radar observations. *Astron. J.* **100**, 1369–1374 (1990).
22. Goldreich, P. & Peale, S. Spin-orbit coupling in the solar system. *Astron. J.* **71**, 425–437 (1966).
23. Goldreich, P. & Peale, S. Spin-orbit coupling in the solar system. II. The resonant rotation of Venus. *Astron. J.* **72**, 662–668 (1967).
24. Gold, T. & Soter, S. Atmospheric tides and the resonant rotation of Venus. *Icarus* **11**, 356–366 (1969).
25. Ingersoll, A. P. & Dobrovolskis, A. R. Venus' rotation and atmospheric tides. *Nature* **275**, 37–38 (1978).
26. Dobrovolskis, A. R. & Ingersoll, A. P. Atmospheric tides and the rotation of Venus. I. Tidal theory and the balance of torques. *Icarus* **41**, 1–17 (1980).
27. Correia, A. C. M. & Laskar, J. The four final rotation states of Venus. *Nature* **411**, 767–770 (2001).
28. Bills, B. G. Variations in the rotation rate of Venus due to orbital eccentricity modulation of solar tidal torques. *J. Geophys. Res.* **110**, E11007 (2005).
29. Hide, R., Birch, N. T., Morrison, L. V., Shea, D. J. & White, A. A. Atmospheric angular momentum fluctuations and changes in the length of the day. *Nature* **286**, 114–117 (1980).
30. Lebonnois, S. et al. Superrotation of Venus' atmosphere analyzed with a full general circulation model. *J. Geophys. Res. Planets* **115**, E06006 (2010).
31. Cottereau, L., Rambaux, N., Lebonnois, S. & Souchay, J. The various contributions in Venus rotation rate and LOD. *Astron. Astrophys.* **531**, A45 (2011).
32. Parish, H. F. et al. Decadal variations in a Venus general circulation model. *Icarus* **212**, 42–65 (2011).
33. Margot, J.-L. A data-taking system for planetary radar applications. *J. Astron. Instrum.* **10**, 2150001 (2021).

34. Margot, J.-L., Peale, S. J., Jurgens, R. F., Slade, M. A. & Holin, I. V. Large longitude libration of Mercury reveals a molten core. *Science* **316**, 710–714 (2007).
35. Margot, J.-L. Mercury's moment of inertia from spin and gravity data. *J. Geophys. Res. Planets* **117**, E00L09 (2012).
36. Stark, A. et al. First MESSENGER orbital observations of Mercury's librations. *Geophys. Res. Lett.* **42**, 7881–7889 (2015).
37. Bendat, J. S. & Piersol, A. G. *Random Data: Analysis and Measurement Procedures* 2nd edn (Wiley, 1986).
38. Correia, A. C. M., Laskar, J. & Néron de Surgy, O. Long-term evolution of the spin of Venus: I. theory. *Icarus* **163**, 1–23 (2003).
39. Correia, A. C. M. & Laskar, J. Long-term evolution of the spin of Venus: II. numerical simulations. *Icarus* **163**, 24–45 (2003).
40. Gross, R. in *Treatise on Geophysics* 1st edn (ed. Schubert, G.) 239–294 (Elsevier, 2007).
41. Goldreich, P. & Peale, S. J. Resonant rotation for Venus? *Nature* **209**, 1117–1118 (1966).
42. Navarro, T., Schubert, G. & Lebonnois, S. Atmospheric mountain wave generation on Venus and its influence on the solid planet's rotation rate. *Nat. Geosci.* **11**, 487–491 (2018).
43. Fukuhara, T. et al. Large stationary gravity wave in the atmosphere of Venus. *Nat. Geosci.* **10**, 85–88 (2017).
44. Kouyama, T. et al. Topographical and local time dependence of large stationary gravity waves observed at the cloud top of Venus. *Geophys. Res. Lett.* **44**, 12098–12105 (2017).
45. Mitchell, J. L. Coupling convectively driven atmospheric circulation to surface rotation: evidence for active methane weather in the observed spin rate drift of Titan. *Astrophys. J.* **692**, 168–173 (2009).
46. Green, P. E. *Radar Astronomy Measurement Techniques* Technical Report No. 282 (MIT Lincoln Laboratory, 1962).
47. Green, P. E. in *Radar Astronomy* (eds Evans, J. V. & Hagfors, T.) Ch. Radar Measurements (McGraw-Hill, 1968).
48. Kholin, I. V. Spatial-temporal coherence of a signal diffusely scattered by an arbitrarily moving surface for the case of monochromatic illumination. *Radiophys. Quant. Elec.* **31**, 371–374 (1988).
49. Kholin, I. V. Accuracy of body-rotation-parameter measurement with monochromatic illumination and two-element reception. *Radiophys. Quant. Elec.* **35**, 284–287 (1992).
50. Margot, J. L., Hauck, S. A., Mazarico, E., Padovan, S. & Peale, S. J. in *Mercury: The View after MESSENGER* (eds Solomon, S. C. et al.) 85–113 (Cambridge Univ. Press, 2018).
51. Duan, X., Moghaddam, M., Wenkert, D., Jordan, R. L. & Smrekar, S. E. X band model of Venus atmosphere permittivity. *Radio Sci.* **45**, 1–19 (2010).
52. Dziewonski, A. M. & Anderson, D. L. Preliminary reference Earth model. *Phys. Earth Planet. Inter.* **25**, 297–356 (1981).
53. Press, W. H., Teukolsky, S. A., Vetterling, W. T. & Flannery, B. P. *Numerical Recipes in C* 2nd edn (Cambridge Univ. Press, 1992).
54. Williams, P. K. G., Clavel, M., Newton, E. & Ryzhkov, D. *pwkit: Astronomical Utilities in Python* ascl:1704.001 (2017).

Acknowledgements

This article is dedicated to the memory of Raymond F. Jurgens, who was instrumental in acquiring the data for this work. We thank M. A. Slade, J. T. Lazio, T. Minter, K. O'Neil and F. J. Lockman for assistance with scheduling the observations. We thank B. A. Archinal, P. M. Davis, S. Lebonnois, J. L. Mitchell and C. F. Wilson for useful comments and A. Lam for assistance with Fig. 1. The Green Bank Observatory is a facility of the National Science Foundation operated under cooperative agreement by Associated Universities, Inc. Part of this work was supported by the Jet Propulsion Laboratory, operated by Caltech under contract with NASA. We are grateful for NASA's Navigation and Ancillary Information Facility software and data kernels, which greatly facilitated this research. J.-L.M. was funded in part by NASA grant nos. NNG05GG18G, NNX09AQ69G, NNX12AG34G and 80NSSC19K0870.

Author contributions

J.-L.M. conducted the investigation and wrote the software and manuscript. D.B.C. contributed to the methodology. J.D.G., J.S.J., L.G.S., F.D.G. and A.B. contributed to data acquisition. All authors reviewed and edited the manuscript.

Competing interests

The authors declare no competing interests.

Additional information

Extended data is available for this paper at https://doi.org/10.1038/s41550-021-01339-7.

Supplementary information The online version contains supplementary material available at https://doi.org/10.1038/s41550-021-01339-7.

Correspondence and requests for materials should be addressed to J.-L.M.

Peer review information *Nature Astronomy* thanks Alexandre Correia, Attilio Rivoldini and the other, anonymous, reviewer(s) for their contribution to the peer review of this work.

Reprints and permissions information is available at www.nature.com/reprints.

Publisher's note Springer Nature remains neutral with regard to jurisdictional claims in published maps and institutional affiliations.

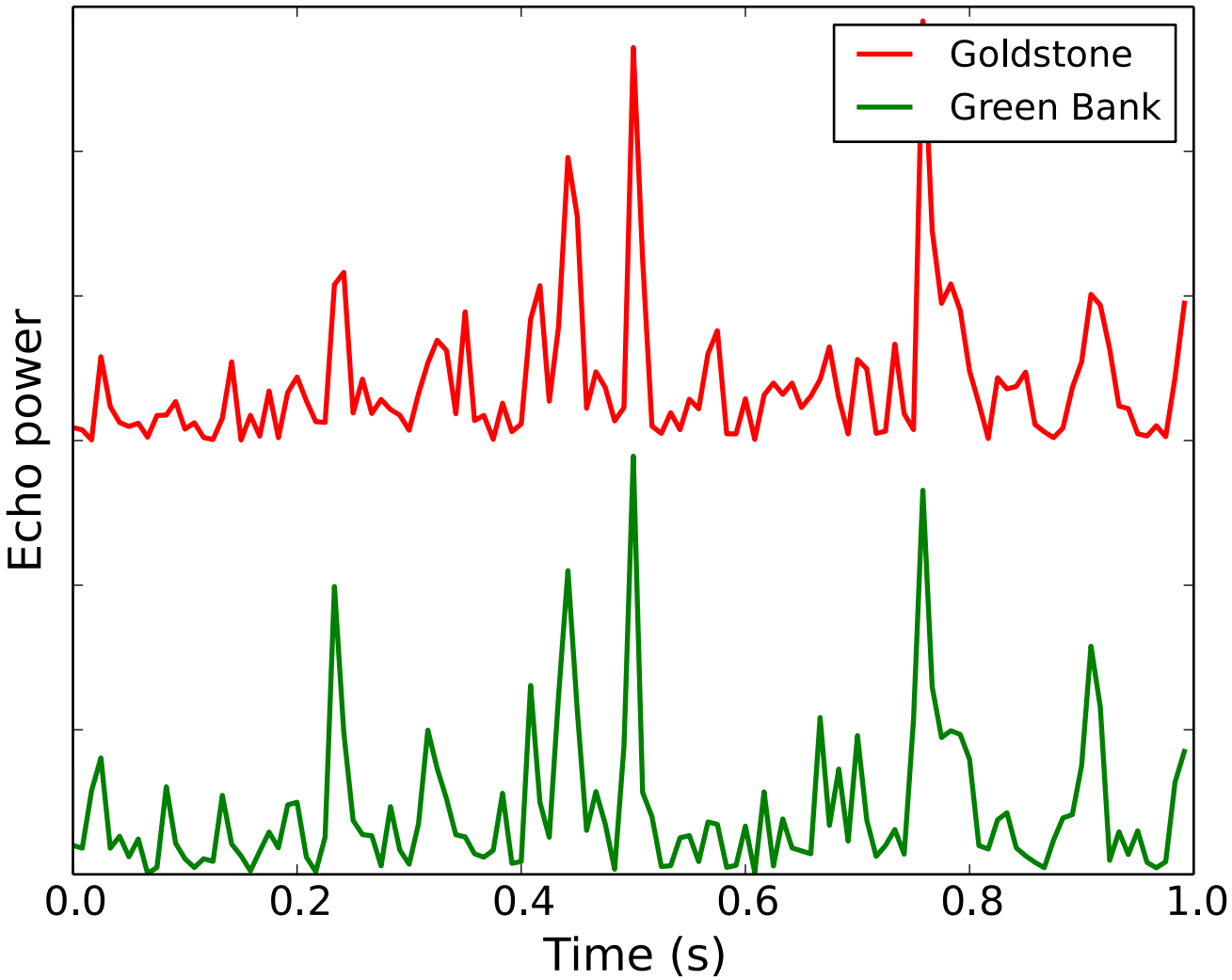

Extended Data Fig. 1 | Random-like variations in radar echo power are illustrated. Representative variations in radar echo power (*speckles*) from observations of Venus with the Goldstone Solar System Radar and Green Bank Telescope at 8560 MHz on 2016 Nov. 26. The GBT echo was shifted in time by 20 s to illustrate the high degree of correlation between the received waveforms when the speckle trajectory is aligned with the antenna baseline.

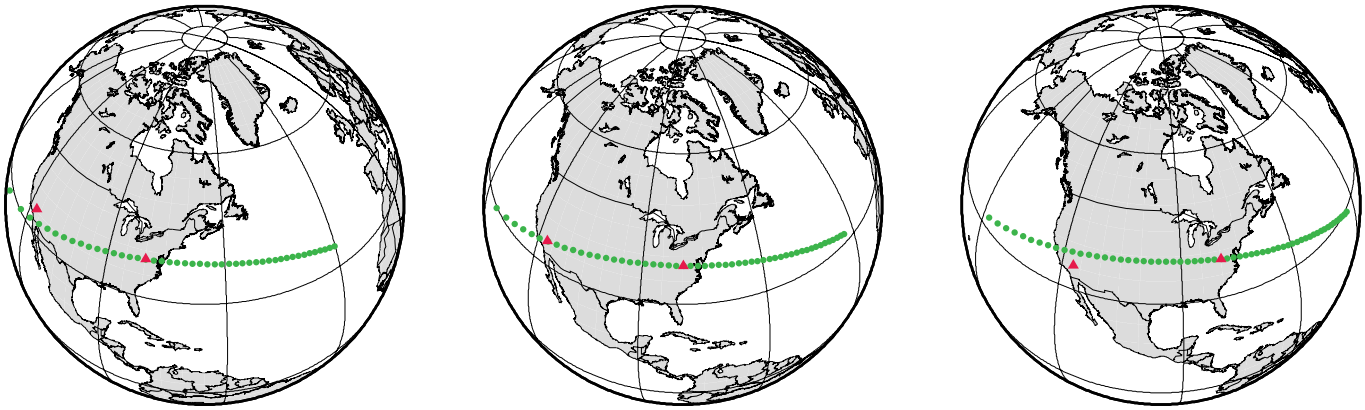

Extended Data Fig. 2 | The trajectory of wavefront corrugations sweeping over both the Goldstone and Green Bank antennas is illustrated. Radar echoes from Venus sweep over the surface of the Earth during the 2020 Sept. 08 observations. Diagrams show the trajectory of the speckles one hour before (left), during (center), and one hour after (right) the epoch of maximum correlation. Echoes from two receive stations (red triangles) exhibit a strong correlation when the antennas are suitably aligned with the trajectory of the speckles (green dots shown with a 1~s time interval).

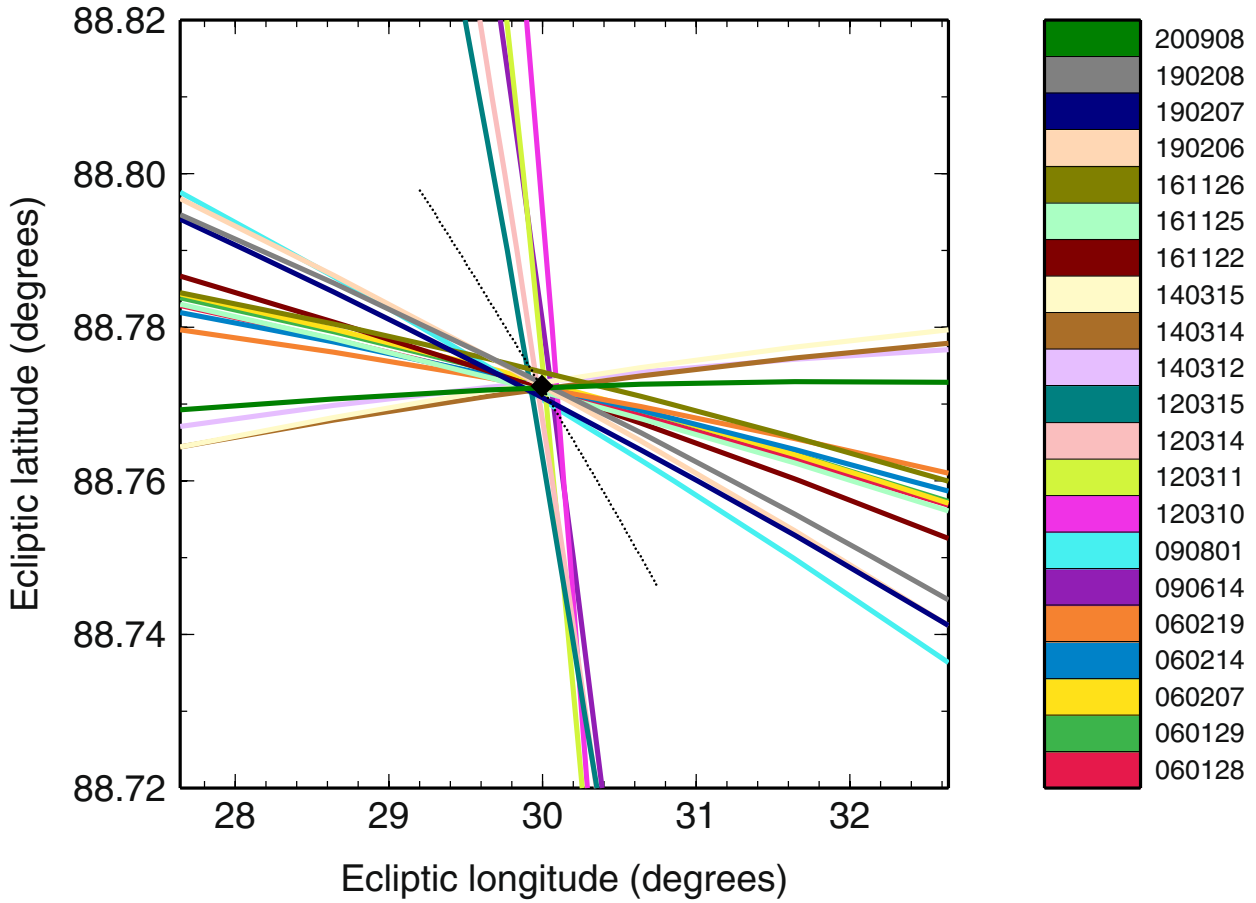

Extended Data Fig. 3 | The constraints on the spin axis orientation of Venus obtained with Goldstone-GBT observations of radar speckles are illustrated. Each colored line represents a measurement of the epoch of correlation maximum that traces a narrow error ellipse on the celestial sphere. The orientation of each line is related to the ecliptic longitude of the projected baseline at the time of observations (Supplementary Table 2). The best-fit spin axis orientation is shown by a diamond at the intersection of the colored lines. All measurements have been precessed to the J2000.0 epoch. The black dotted line represents the trace of the spin axis orientation on the celestial sphere as a result of spin precession between 1950 and 2050.

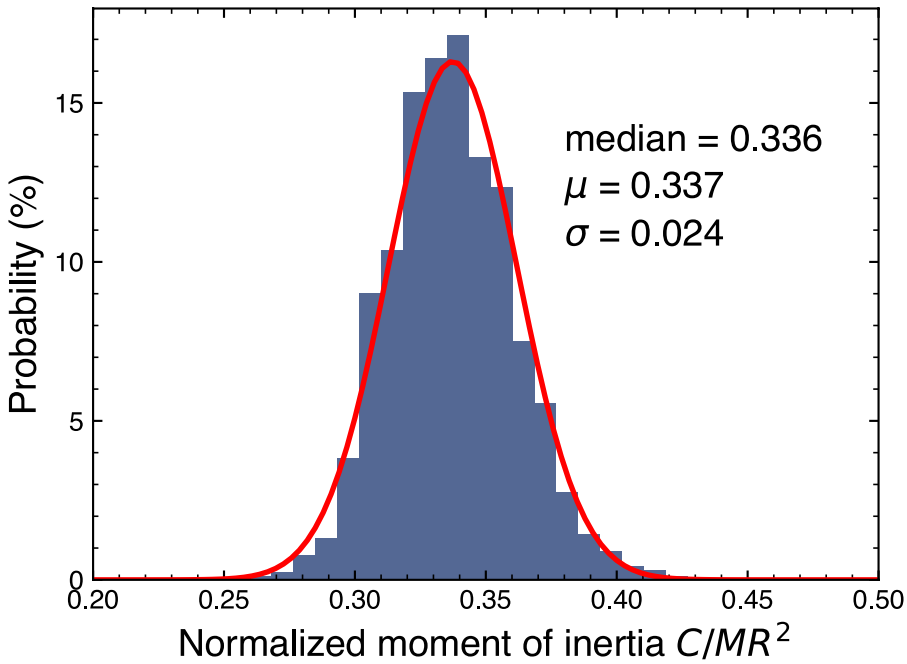

Extended Data Fig. 4 | The distribution of normalized moments of inertia from the bootstrap analysis is illustrated. Radar speckle tracking estimates of the normalized moment of inertia of Venus suggest residual uncertainties of 7% with the data obtained to date.